C. R. Chimie 21 (2018) 327–338

Contents lists available at ScienceDirect

Comptes Rendus Chimie

www.sciencedirect.com

Full paper/Mémoire

Optical and electrochemical-mediated detection of ascorbic acid using manganese porphyrin and its gold hybrids

Iuliana Sebarchievici [a], Anca Lascu [b], Gheorghe Fagadar-Cosma [c], Anca Palade [b], Ionela Fringu [b], Mihaela Birdeanu [a], Bogdan Taranu [a], Eugenia Fagadar-Cosma [b, *]

[a] National Institute for Research and Development in Electrochemistry and Condensed Matter, 1, Plautius Andronescu Street, 300224 Timisoara, Romania
[b] Institute of Chemistry Timisoara of Romanian Academy, M. Viteazul Avenue 24, 300223 Timisoara, Romania
[c] Politehnica University of Timisoara, Faculty of Industrial Chemistry and Environmental Engineering, Victoriei Square 2, 300006 Timisoara, Romania

ARTICLE INFO

Article history:
Received 2 March 2017
Accepted 13 July 2017
Available online 23 August 2017

Keywords:
Mn porphyrin
Gold colloid
Hybrid nanomaterial
Modified GC electrodes
Ascorbic acid detection
Electrocatalytic effect

ABSTRACT

The developments concerning new hybrids based on porphyrin derivatives and colloids destined for the detection of ascorbic acid (AA) in the relevant range for medical investigations are presented. Mn(III) tetratolylporphyrin chloride (MnTTPCl), spherical gold colloid (n-Au), and their hybrid (MnTTPCl/n-Au) were chosen to be comparatively investigated by ultraviolet–visible spectroscopy in the presence of AA. The hybrid material (MnTTPCl/n-Au) has the best capacity to detect concentrations of AA in the range of 2.6×10^{-6}–4.38×10^{-5} M. Modified glassy carbon (GC) electrodes were obtained by thin film deposition of MnTTPCl, n-Au alone, and in successive mixed thin films, comparing their response during the electrochemical oxidation of AA. The electrocatalytic effect of the MnTTPCl on the AA oxidation is justified both by the increase in the peak current density and by the shift toward more negative potentials (0.024 V). The GC/MnTTPCl electrode has the best electrocatalytic effect for the AA oxidation and is promising for sensor applications.

1. Introduction

Ascorbic acid (AA) is known for its antioxidant properties. It is used for the prevention and treatment of several illnesses, such as immune response activation, mental illnesses, infertility, cancers, and AIDS [1], and is responsible for neuroprotection [2], iron absorption and hematopoiesis, and vascular system integrity [3,4]. Actual treatments recommend a rich diet in hydrosoluble AA that can bring health benefits due to its capacity to be readily oxidized to dehydroascorbic acid [5,6].

The normal amount of AA contained in human biological fluids (plasma) can vary from as little as 16.8 μmol/L [7] to as much as 25–30 mmol/L, representing the maximum curative dose, because the excess in AA can provoke gastric irritation and renal problems [8]. On the other hand, a deficiency in the AA antioxidant favors the incidence of cardiovascular disease [7] and can affect the patients with porphyria cutanea tarda [9,10].

Besides, AA can be used to determine the oxidative stress [11] in human metabolism, which is linked to diabetes, cancer, and hepatic diseases. The detection method based on metaphosphoric acid shows that significant higher levels of AA are found in women: 56.4 ± 19.8 μmol/L in women versus only 46.2 ± 23.5 μmol/L in men [12,13].

* Corresponding author.
E-mail address: efagadar@yahoo.com (E. Fagadar-Cosma).

http://dx.doi.org/10.1016/j.crci.2017.07.006
1631-0748/

For the determination of AA in aqueous solutions, a new spectrophotometric method was developed, based on its ability to reduce the colors of $KMnO_4$ and $K_2Cr_2O_7$ [14]. By this method, the concentration range of detectable AA is in the parts per million region.

A recent colorimetric method for AA trace analysis is based on the ink-jet printing technique using as reagent dye the 2,2′-bipyridyl-Fe^{+3} (bipy-Fe^{+3}) complex, immobilized in a Nafion matrix [15]. Other studies were concerned on AA detection using graphene flowers [16], highly photoluminescent nitrogen-doped carbon nanoparticles providing excellent sensitivity and selectivity from 0.2 to 150 μM [17], and on ratiometric electrochemical sensors [18].

Porphyrin-based amperometric and potentiometric sensors for the detection of electroactive analytes are based on electrochemical oxidation or reduction of these analytes, mediated by a specific redox couple of metalloporphyrin films [19]. Fe porphyrin, creating a hybrid with aniline, proved to have an electrocatalytic effect toward the electro-oxidation of AA that is more active than the polyaniline because the oxidation potential is shifted to less positive values.

For the electrochemical determination of dopamine and AA, a simultaneous voltammetric determination on a modified carbon paste electrode prepared with 5,10,25,20-tetraphenylporphyrin iron(III) chloride immobilized on niobium oxide grafted on a silica gel surface (SiO_2/Nb_2O_5) inorganic matrix [20]. The detection range for AA in case of this electrode is very limited from 1.0×10^{-4} to 8.0×10^{-4} mol/L.

Modified glassy carbon (GC) electrodes with *meso*-tetraphenylporphyrin iron(III) chloride and Cameroonian smectite clay have been prepared [21] and used for simultaneous detection of AA, uric acid, and nitrite. The same compounds in urine and serum samples were successfully detected using modified electrodes with multiwalled carbon nanotubes functionalized with iron(III) porphyrin [1].

The rich redox-based chemistry of manganese porphyrins is responsible for their ability to affect signaling processes [22]. Manganese *ortho*-tetrakis(*N*-ethylpyridinium-2-yl)porphyrin (MnTE-2-PyP) and manganese *meta*-tetrakis(*N*-ethylpyridinium-3-yl)porphyrin (MnTE-3-PyP) have the capacity to develop in aqueous solutions in the pH limits 2–13, several species with Mn in the oxidation state from II to IV, as follows: (H_2O)Mn(II)TE-*m*-PyP^{4+}, (HO)Mn(II)TE-*m*-PyP^{3+}, (H_2O)2Mn(III)TE-*m*-PyP^{5+}, (HO)(H_2O)Mn(III)TE-*m*-PyP^{4+}, (O)(H_2O)Mn(III)TE-*m*-PyP^{3+}, (O)(H_2O)Mn(IV)TE-*m*-PyP^{4+}, and (O)(HO)Mn(IV)TE-*m*-PyP^{3+} (m = 2, 3).

Fluorophotometry was used for the study of the interaction between 5,10,15-triphenyl-20-pyridyl porphyrin and AA [23]. In the presence of cetyltrimethylammonium bromide microemulsion, the absorption and fluorescence intensities of the porphyrin were greatly enhanced. Adding AA causes the quenching effect, that is, in linear dependence with the AA concentration, allowing for its determination in commercial tablets.

The main aim of this work was to compare the AA optical and electrochemical detection capacity of a bare manganese porphyrin derivative, namely, Mn(III) tetratolylporphyrin chloride (MnTTPCl), spherical gold colloid (10–15 nm in diameter) alone, and of the hybrid formed between gold nanoparticles and Mn porphyrin.

2. Materials and methods

2.1. Materials

The used solvents and reagents (THF, AA) were purchased from Merck. 5,10,15,20-Tetra(4-methyl-phenyl) porphyrinato manganese (III) chloride (MnTTPCl) was prepared by metalation of the porphyrin base with a large excess of manganese salts [24]. The free porphyrin was previously synthesized using modified Adler's method [25] and fully characterized [26], and the gold colloid with spherical dimensions in a narrow range was synthesized in an environmentally friendly manner [27].

2.2. Methods

Spectrophotometric measurements were performed in 1 cm wide quartz cuvettes using a JASCO model V-650 spectrometer. For the registration of atomic force microscopy (AFM) images a Nanosurf EasyScan2 Advanced Research AFM (Switzerland) microscope was used. The samples were deposited from THF and water mixtures onto pure silica plates and the surface imaging was performed at room temperature. AFM images were obtained in noncontact mode.

Scanning transmission electron microscopy (STEM) images were recorded using a Titan G2 80-200 TEM/STEM microscope (FEI Company, The Netherlands). Samples were prepared by drop-casting the MnTTPCl/n-Au hybrid with and without AA from THF–water mixtures on 200 mesh TEM copper grids coated with continuous carbon film. The images were registered at 200 kV using TEM Imaging and Analysis v. 4.7 software.

Electrochemical investigations were performed using a VoltaLab PGZ 301 potentiostat (Radiometer). A three-electrode conventional cell equipped with saturated calomel electrode (SCE) as reference electrode, a Pt wire as auxiliary electrode, and bare GC ($S = 0.07$ cm^2) or modified GC with MnTTPCl, nAu, or MnTTPCl/n-Au hybrid as working electrodes was used.

2.3. Experimental section

2.3.1. Obtaining of the MnTTPCl/n-Au hybrid

With the purpose to exhibit the highest plasmon intensity a complex between gold colloid and MnTTPCl was obtained as follows: 0.5 mL of a MnTTPCl solution in THF (1×10^{-6} M) was added to a 6 mL gold colloid solution (4.58×10^{-4} M) in water under vigorous stirring at room temperature.

The ultraviolet–visible (UV–vis) spectra of the gold colloid, Mn porphyrin, and of the hybrid (MnTTPCl/n-Au) are presented in Fig. 1. In the inset of Fig. 1 the UV–vis spectrum of AA solution in water is presented.

2.3.2. General procedure for detection of AA by the MnTTPCl/n-Au hybrid, bare manganese porphyrin, and spherical gold colloid alone

Portions of 20 μL of an AA solution (6.5×10^{-4} M) in doubly distilled water were successively added to 5 mL of each investigated solution (MnTTPCl/n-Au hybrid, bare MnTTPCl in THF, and bare gold colloid solution) under stirring. After 30 s, the UV–vis spectrum was recorded for each sample.

2.3.3. Electrochemical investigations. Modification of GC electrodes with thin films of MnTTPCl and gold

The method for preparation of the modified GC electrodes is completely described in our previous publication [28]. The deposition of the MnTTPCl film on the surface of GC electrode was performed both by drop-casting from DMF solution (GC/MnTTP) and by electrochemical stepwise scanning of 5, 10, and 20 cycles (GC/5cycl.MnTTP, GC/10cycl.MnTTP, and GC/20cycl.MnTTP).

3. Results and discussions

The main purpose of this work was to realize a more facile and readily usable method to detect and quantify AA vitamin in aqueous solutions by spectrophotometric detection. The electrochemical study was also performed to certify the electrocatalytic effect of MnTTPCl upon the oxidation of AA on modified GC electrodes.

3.1. UV–vis analysis

The overlapped UV–vis spectra represented in Fig. 1 clearly put into evidence the differences between the green MnTTPCl solution in THF (curve 1), the red gold colloid solution (curve 2), and the MnTTPCl/n-Au hybrid (curve 3). The inset represents the UV–vis spectrum of the AA solution in water. Distinctive major peaks of band V (called also Soret) positioned at 476 and 532 nm are characteristic for the Mn porphyrin and the gold colloid plasmon.

The plasmonic band of the MnTTPCl/n-Au hybrid has the aspect of a large plateau and is significantly red shifted to 664 nm, and enlarged in the wavelength range of 480–850 nm, due to charge transfer that enrich resonance in the MnTTPCl/n-Au complex. In the presence of n-Au, the static and dynamic optical properties of the porphyrin macrocycle change systematically with the distortion of planarity. So, the optical spectra of nonplanar porphyrin/n-Au hybrid are shifted to absorption at lower energy when compared to planar porphyrins [29,30] These two properties make the MnTTPCl/n-Au hybrid special for applications in medicine (Photodynamic Therapy of Cancer [PDT]) and technical uses (catalysis and photovoltaic cells).

The hybrid between MnTTPCl and gold nanoparticles was treated with increasing quantities of AA, as described, while measuring the intensity of absorption (Fig. 2).

The addition of the acid to the MnTTPCl/n-Au hybrid produces a red shift in the plasmon intensity (Fig. 2), from 664 nm in the MnTTPCl/n-Au hybrid to 682 nm due to the host–guest interaction process between manganese core of the porphyrin and AA.

It can be observed that the intensity of the plasmonic band of the MnTTPCl/n-Au hybrid decreases in a linear fashion as the AA concentration increases. The dependence between the UV–vis intensity of the MnTTPCl/n-Au hybrid and the AA concentration is characterized by an excellent correlation coefficient of 99.19% (Fig. 3). The presence of one clear isosbestic point in the UV–vis spectra at 808 nm wavelength (Fig. 2 inset) indicates the existence of only one equilibrium process in the whole range of concentrations.

The lowest AA concentration detected by the hybrid solution was 2.6×10^{-6} M and the highest exceeded one order of magnitude, being 4.38×10^{-5} M (Fig. 3).

A second aim of the work was to compare the MnTTPCl/n-Au hybrid behavior with its components in the process of AA detection.

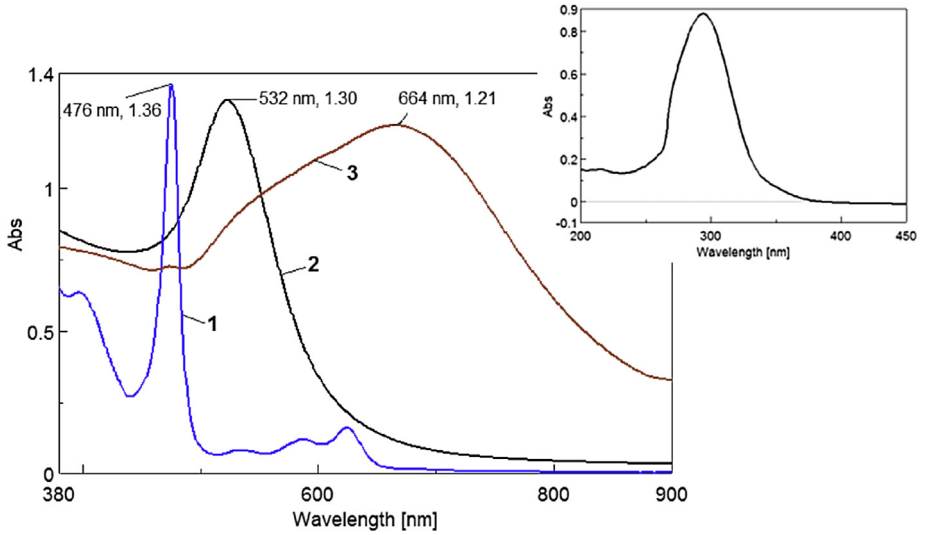

Fig. 1. UV–vis spectra of the MnTTPCl solution in THF (1×10^{-6} M) (curve 1), the gold colloid solution (4.58×10^{-4} M) (curve 2), and the MnTTPCl/n-Au hybrid (curve 3). Inset represents the UV–vis spectrum of the AA solution in water ($c = 6.529 \times 10^{-4}$ M).

In the second case of adding AA to bare manganese porphyrin in THF solution, it can be noticed that for low concentrations of AA (2.6×10^{-6}–1.7×10^{-5} M) the Soret band intensity is randomly dispersed (Fig. 5) and hypsochromically shifted to 469 nm. The isosbestic point at 475 nm (Fig. 5a, Soret band) indicates the formation of an intermediate Mn(IV) compound. In the UV–vis Q bands (Fig. 5b), a second isosbestic point is obvious at 617 nm, which cannot be attributed to the increasing acidity, because the QIII band located around 625 nm has no tendency to increase its intensity and to shift toward higher wavelengths. We presume that this second isosbestic presence is linked to the generation of O═Mn(V) species. As a consequence, a complex between AA and the manganese porphyrin (Fig. 4) is more likely to occur in the same way as previously reported [31]. Besides, manganese is well known for its capacity to modify its oxidation state and for its affinity to oxygen atoms. In addition, these changes were put into evidence on Fourier transform infrared (FT-IR) spectra, discussed in Section 3.2.

The further adding of AA to the complex leads to the increase in the intensity of the Soret band and to the continuous shift to lower wavelengths (final registered AA concentration 4.9×10^{-5} M located at 469 nm). The correlation between the Soret band intensity and the AA concentration for the narrow concentration domain 1.7×10^{-5}–4.9×10^{-5} M is ascending and linear. This dependence between the UV–vis intensity of the Soret band and the AA concentration is characterized by an excellent correlation coefficient of 99.17% (Fig. 6).

In the third case of pure gold colloid solution treated with diluted AA solution, it can be concluded that the AA does not influence the shape or the wavelength of the gold plasmon absorption intensity (Fig. 1), the only visible effect being that of dilution (Fig. 7).

3.2. FT-IR analysis

The FT-IR band around 1385 cm^{-1} in the spectrum of MnTTPCl (Fig. 8, curve 1) was assigned to symmetric stretching of pyrrole half-ring vibrations (C–N) from the porphyrin ring. The bands in the range 1250–1280 cm^{-1} were assigned to C_m-phenyl. Pyrrole vibration δ(C–H) is responsible for the strong and sharp band from 1005 cm^{-1}. The two high intensity bands located around 750 and 800 cm^{-1} were assigned to rotations and out of plane vibrations of porphyrin macrocycle and γC–H from pyrrole rings.

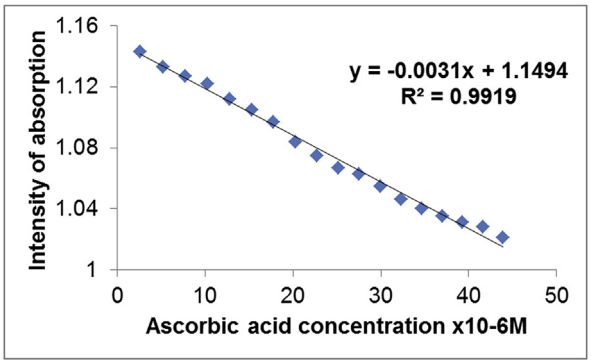

Fig. 3. Correlation coefficient between the intensity of absorption of the plasmonic band of the MnTTPCl/n-Au hybrid and the AA concentration.

The overlapped IR spectra of the investigated materials show that the C–O primary and secondary bonds, characteristic for AA (Fig. 8, curve 2), can be identified as bands at 1058 cm^{-1} both in the complexes formed between the MnTTPCl and AA and MnTTPCl/n-Au hybrid and AA in Fig. 8, curve 5, and Fig. 8, curve 3, respectively. A very intense and sharp band newly located at 902 cm^{-1}, attributed to the ν_{C-O} ring bond, can be the proof for the complex formation between the MnTTPCl and AA. This complex formation is also confirmed by UV–vis behavior [31] (Fig. 4). It can be also observed that the hydrogen bonding broadens and shifts the carbonyl absorption band (1751 cm^{-1} in AA) to shorter wavelengths, at around 1640 cm^{-1} in both materials MnTTPCl and MnTTPCl/n-Au treated with AA. This band is also amplified by the contribution of C═C bond

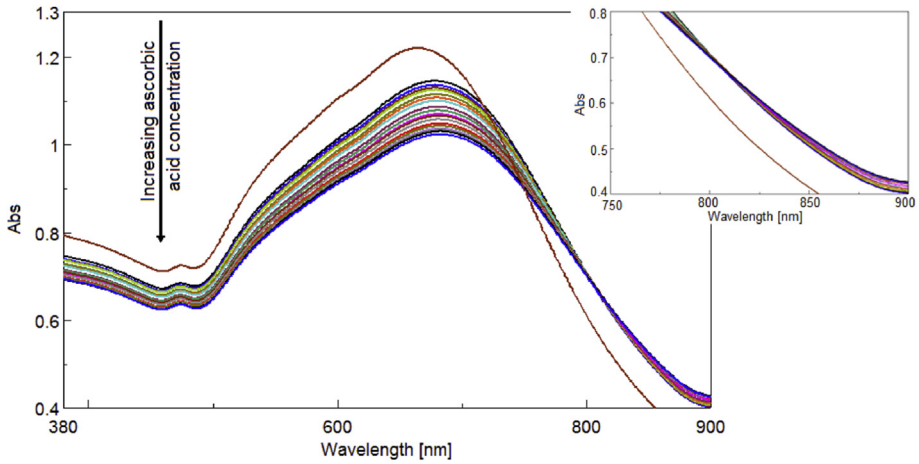

Fig. 2. Superimposed UV–vis spectra recorded after adding of AA to the MnTTPCl/n-Au hybrid solution. Inset: isosbestic point in the UV–vis spectra at 808 nm wavelength.

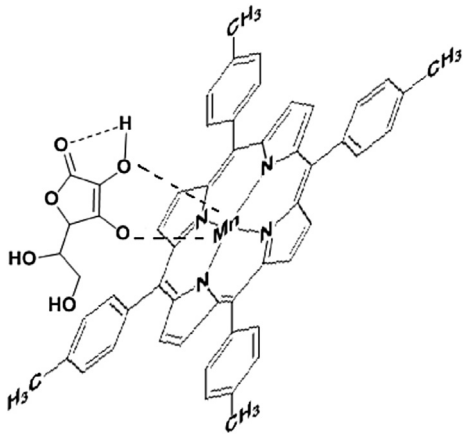

Fig. 4. The host–guest interaction between manganese core of the porphyrin and AA.

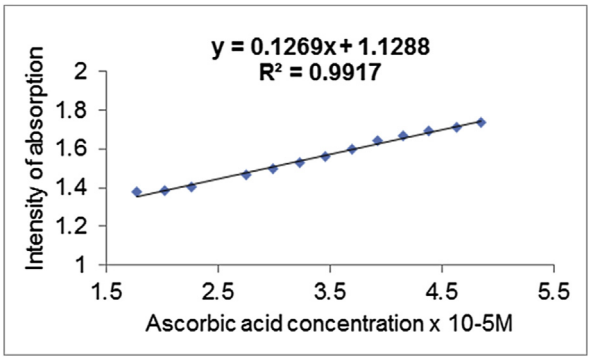

Fig. 6. Correlation coefficient between the intensity of absorption of the Soret band at concentrations of AA in the range 1.7×10^{-5}–4.9×10^{-5} M.

stretching characteristic for the aromatic cycle, as a contribution of the porphyrin moiety. The bands around 2860–2960 cm^{-1}, characteristic for C–H bond stretching, are also present in the samples that contain porphyrin. The O–H characteristic absorption band at around 3400 cm^{-1} is present in all liquid samples.

The gold colloid spectrum (curve 4 in Fig. 8) presents the characteristic small bands around 1450 and 1250 cm^{-1} but also the intense absorption band from 1600 cm^{-1}. According to the literature data [32], the bands of the gold nanoparticles can be also identified in the gold hybrid complexes.

3.3. AFM analysis

The AFM images of MnTTPCl/n-Au show evidence for the H- and J-type aggregation. The ordered triangular shaped particles with dimensions in the range of 160–285 nm are evenly distributed (Fig. 9a). This organization is no longer visible in the case of the MnTTPCl/n-Au hybrid treated with AA (Fig. 9b). In this situation the particles are decreasing in size to a maximum 130 nm, became spherical, and completely losing their triangular shape. The height distribution of the particles is between 3 and 6 nm for the porphyrin–gold hybrid (Fig. 9c) and in the range of 35–55 nm for the hybrid exposed to AA (Fig. 9d).

The measured rugosity is decreasing from Sa = 9.9 nm in case of MnTTPCl/n-Au hybrid to Sa = 1.2 nm in the case of the hybrid treated with vitamin C. The presence of AA

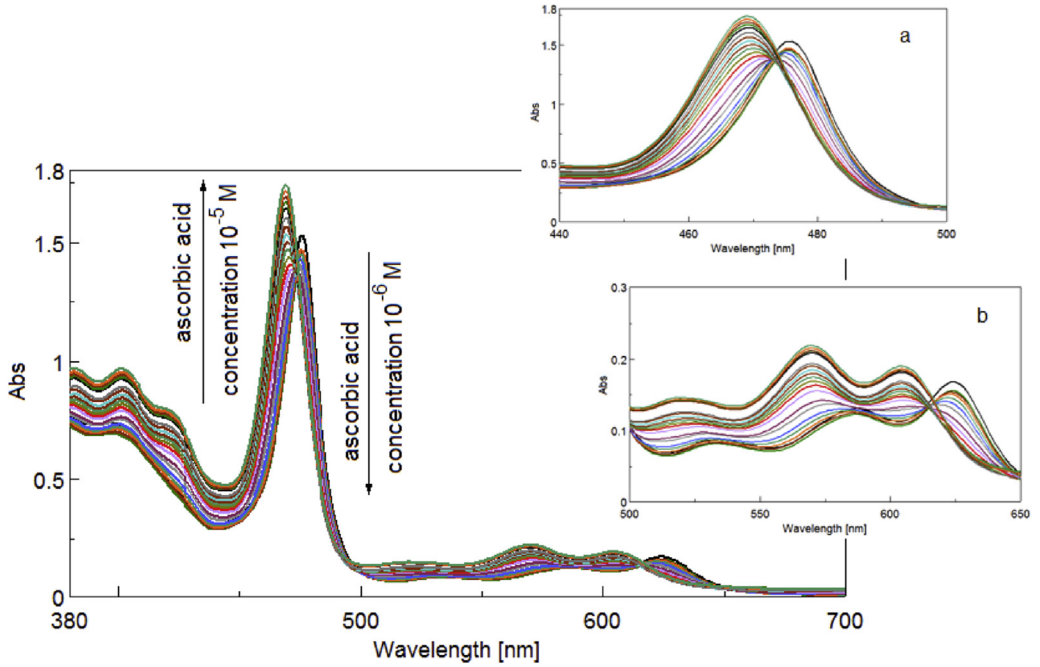

Fig. 5. Overlapped spectra for the adding of AA solution to the MnTTPCl solution in THF ($c = 1.1 \times 10^{-6}$ M). Soret band region (a) and Q band region (b).

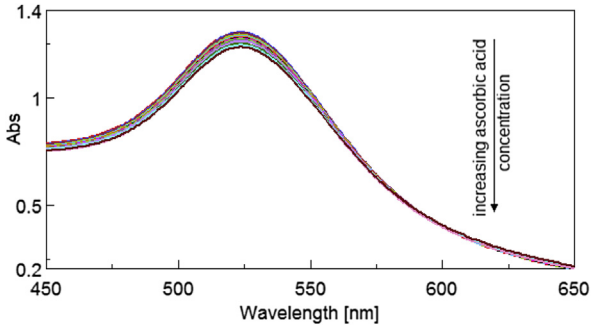

Fig. 7. Overlapped UV–vis spectra for the adding of AA solution to gold colloid solution ($c = 4.58 \times 10^{-4}$ M).

influences the morphology of the surface, producing uniformly deposited thicker layers.

3.4. STEM analysis

By comparing the images recorded for the MnTTPCl/n-Au hybrid with those obtained for the same hybrid in the presence of AA, clear differences can be observed. In the absence of AA, the Au nanoparticles tend to organize into circular clusters, whereas the MnTTPCl molecules form an inhomogeneous film (Fig. 10a and c).

The STEM images obtained for the samples containing AA (Fig. 10b, d, and e) show a higher degree of dispersion for the gold nanoparticles that no longer formed circular structures. The interaction between MnTTPCl and the AA resulted in the formation of flat ovoid aggregates with lacey edges having dimensions of up to 500 nm.

3.5. MnTTPCl as electrochemical mediator for the oxidation of AA on modified GC electrodes

3.5.1. GC electrode modified with MnTTPCl by drop-casting

The capacity of manganese to exist in various oxidation states is well known; therefore, the Mn porphyrins possess high redox versatility [33]. Mn(III)-5,10,15,20-tetrakis(4-methyl-phenyl)porphyrin chloride was deposited in thin films on GC electrodes to investigate the behavior and the response of these modified electrodes to the oxidation of AA.

As can be seen in Fig. 11, in the case of the electrode modified with MnTTPCl by drop-casting the AA oxidation takes place at a more negative potential as compared to the unmodified electrode. Both the current density corresponding to the anodic process and the capacitive currents are lower as compared to the ones registered for the unmodified electrode. The intensity of the oxidation peak increases with the increase in AA concentration. As expected, the presence of the MnTTPCl film leads to an intensification of the current density of the anodic process due to its catalytic capacity.

3.5.2. GC electrode modified with MnTTPCl by electrochemical deposition

In the case of electrochemical deposition of MnTTPCl on GC electrodes, the influence of the number of cycles upon the response of the modified electrodes to the presence of

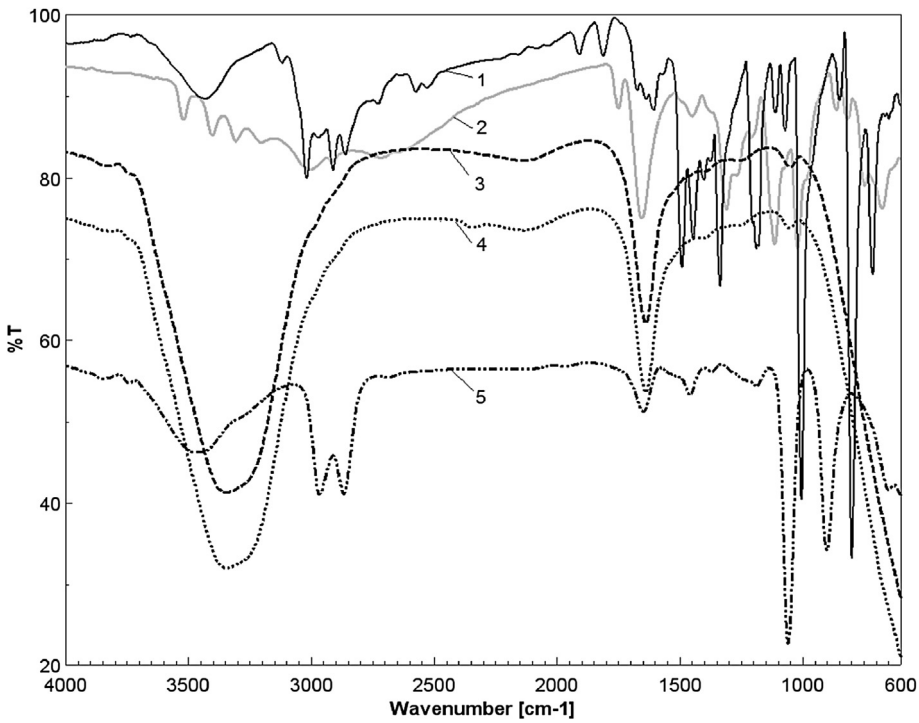

Fig. 8. Overlapped IR spectra: MnTTPCl solution (curve 1); AA (curve 2); complex MnTTPCl/n-AuAA (curve 3); gold colloid (curve 4); and MnTTPCl–AA (curve 5).

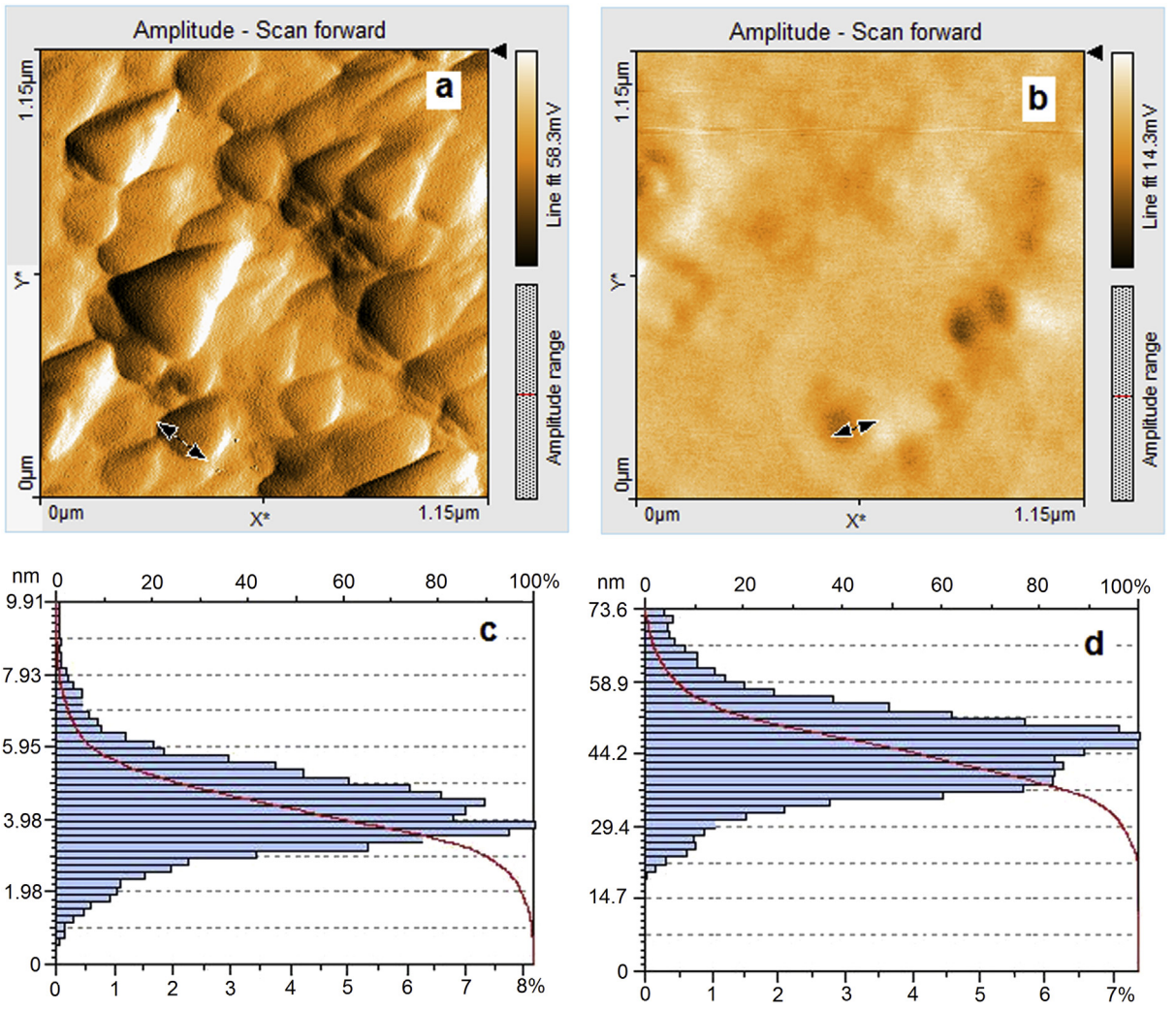

Fig. 9. AFM images and characteristics for MnTTPCl/n-Au hybrid (a and c) and hybrid after treatment with AA (b and d).

AA was studied. Cyclic voltammograms presented in Fig. 12 show the GC electrode behavior during the deposition of the MnTTPCl film in a solution of 0.5 mM MnTTPCl/0.05 M TBAP/DMF for 20 scans. During the scanning in the chosen potential range, the oxidation and reduction peaks corresponding to the porphyrin ring are initially decreasing and then are increasing in intensity as the number of cycles grows. This behavior can be attributed both to the self-aggregation of the adsorbed Mn porphyrin molecules and to the distortion of the planar conformation of the macrocycle. So, the distortion is responsible for the symmetry decrease of porphyrin and also favors the macrocyclic inversion and may control electron-transfer rates by stabilizing certain conformers over others. A distorted porphyrin can also induce unique chemical reactivity of the macrocycle giving enantiomeric selectivity in catalytic reactions [29,30,34,35].

The cathodic peak at −300 mV is continuously increasing. The new peak that appears at 800 mV is also increasing with the number of cycles.

Previously published studies [36] revealed that, in the case of MnTTPCl, two redox couples are present around −0.75 and 0 V that were attributed to the central manganese atom. The same authors certify that the porphyrin ligand oxidation starts at potentials higher than +1.0 V, as can be observed in Fig. 12.

Values for $E_{eq} = 0.02$ V in aqueous solution and −0.1 V in organic solution were established in other studies [37] for the reduction process Mn(III)/Mn(II). Another redox couple at 0.52 V is also mentioned, because of the well known capacity of manganese to generate Mn(III)/oxo-Mn(IV) oxidations [28]. When the peak is situated around 0.95 V it is possible that the Mn oxidation can lead to Mn(V) compounds as well [38].

The UV–vis spectra previously recorded by our group [33] evidenced the presence of isosbestic points located around 340, 420, 450, 500, and 620 nm, proving the following transformations: Mn(III)TTPCl ↔ Mn(II)TPP and Mn(III)TTPCl ↔ O=Mn(IV)TTP accompanied by short life species like O=Mn(V) [39,40].

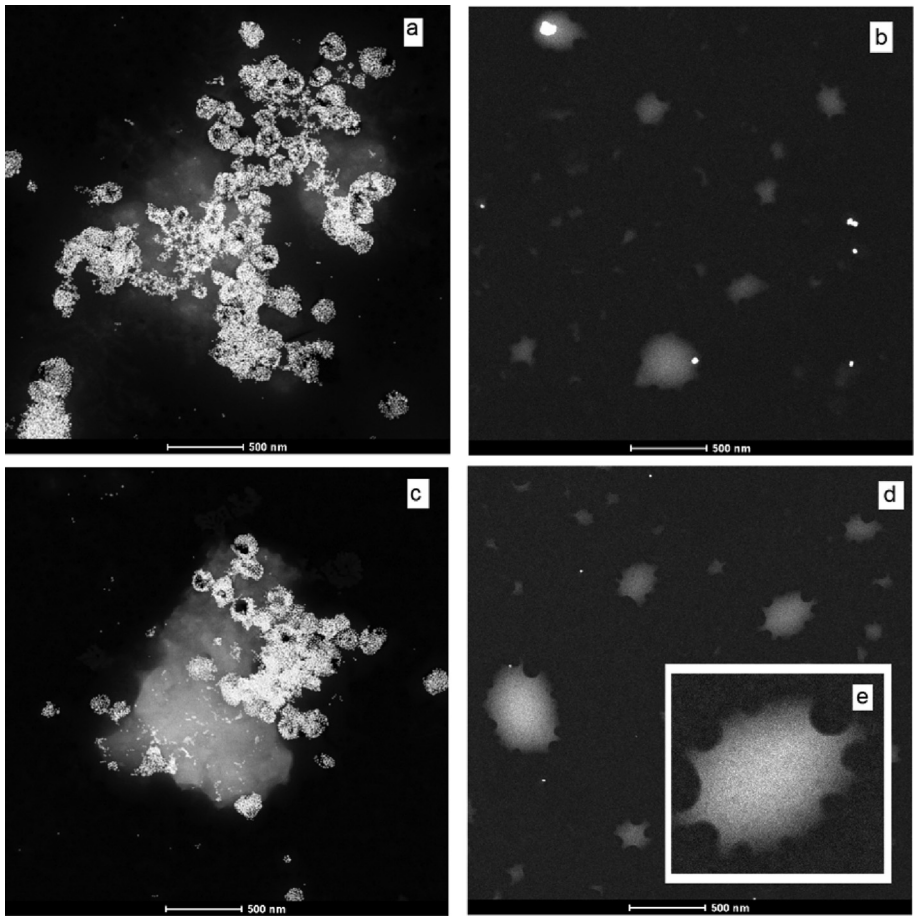

Fig. 10. Images recorded in STEM mode for the MnTTPCl/n-Au hybrid in the absence (a and c) and in the presence of AA (b, d, and inset e).

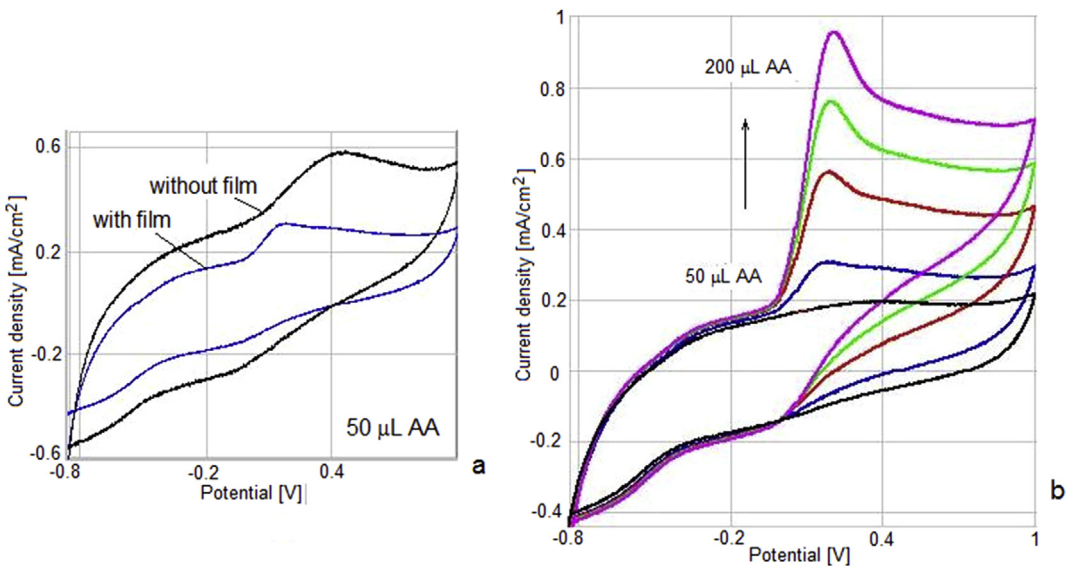

Fig. 11. Cyclic voltammograms in the presence of 2.8 mM AA in 0.1 M phosphate-buffered solution for unmodified GC electrode and for GC/MnTTPCl (a); the response of the GC/MnTTPCl electrode to increasing concentrations of AA: 0, 2.8, 5.6, 8.4, and 11.2 mM (b).

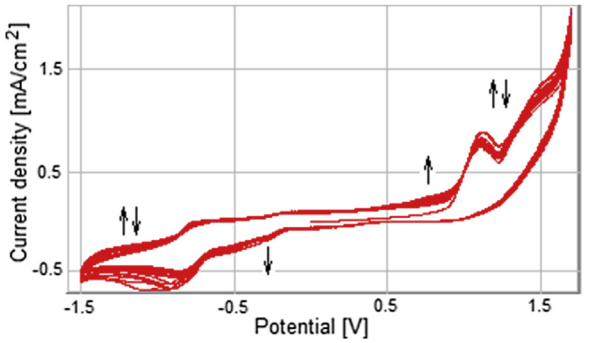

Fig. 12. Cyclic voltammograms of the GC electrode during its modification with Mn porphyrin thin film; 20 cycles; solution of 0.5 mM MnTTPCl/0.05 M TBAP/DMF, v = 100 mV/s.

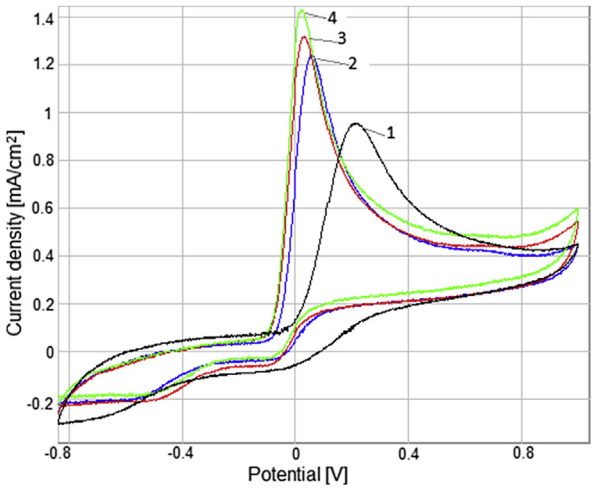

Fig. 13. Cyclic voltammograms of 2.8 mM AA in a phosphate-buffered solution 0.1 M/KCl 0.1 M, scanning rate 100 mV/s, for the unmodified GC electrode (curve 1), modified GC/5cycl. MnTTPCl (curve 2), GC/10cycl.MnTTPCl (curve 3), and GC/20cycl.MnTTPCl (curve 4).

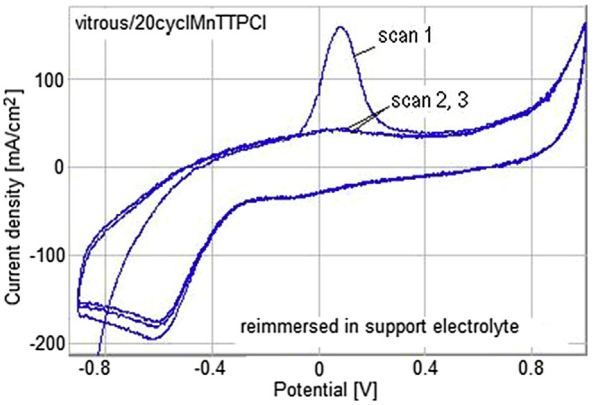

Fig. 15. Reusability of the GC/20cycl.MnTTPCl electrode.

The voltammograms of the modified electrodes using different scan cycles (GC/5cycl. MnTTPCl, GC/10cycl. MnTTPCl, and GC/20cycl.MnTTPCl) in the presence of 2.8 mM AA in phosphate-buffered solution 0.1 M/KCl 0.1 M are presented in Fig. 13. The best response (Fig. 13, curve 4) was provided by the GC/20cycl.MnTTPCl electrode that was chosen for the monitoring of the AA oxidation.

It can be observed that the oxidation of AA takes place in the 24–62 mV potential range in the case of MnTTPCl-modified GC electrodes. The decrease in oxidation potential can be attributed to the increased selectivity of porphyrin-ruffled conformer (the most prevailed deformation of Mn porphyrins [34]) toward binding of AA, thus favoring the oxidation process.

The electrocatalytic effect of the MnTTPCl-modified GC electrodes is justified both by the increase in the peak current density and the shift toward more negative potentials. The voltammetric response of the GC/20cycl.MnTTPCl electrode to increasing concentrations of AA (0.14–14.17 mM) in phosphate-buffered solution 0.1 M/

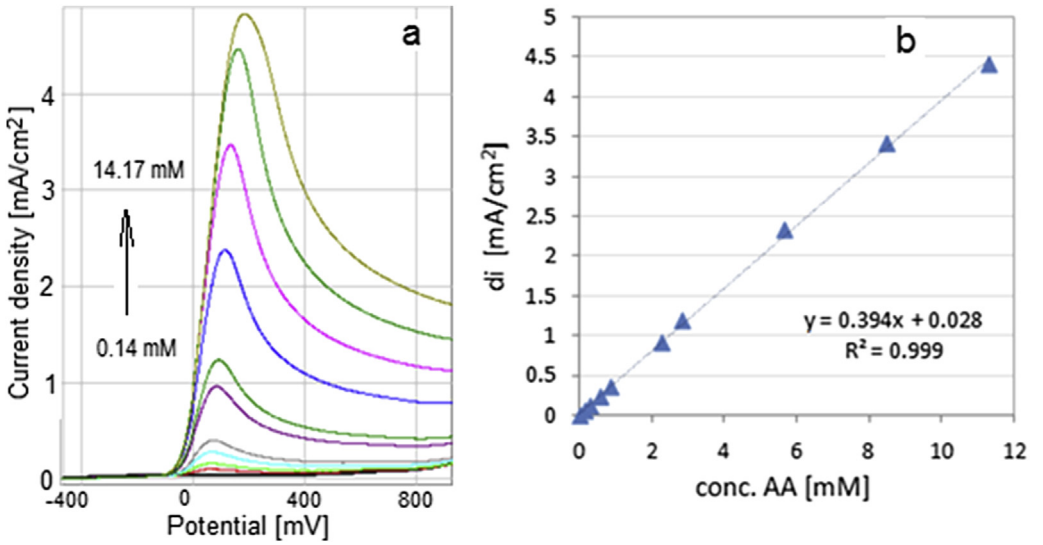

Fig. 14. Voltammetric response of GC/20cycl.MnTTPCl electrode to increasing concentrations of AA in a phosphate-buffered solution 0.1 M/KCl 0.1 M (a); the dependence between the density of anodic current (di) and AA concentration (b).

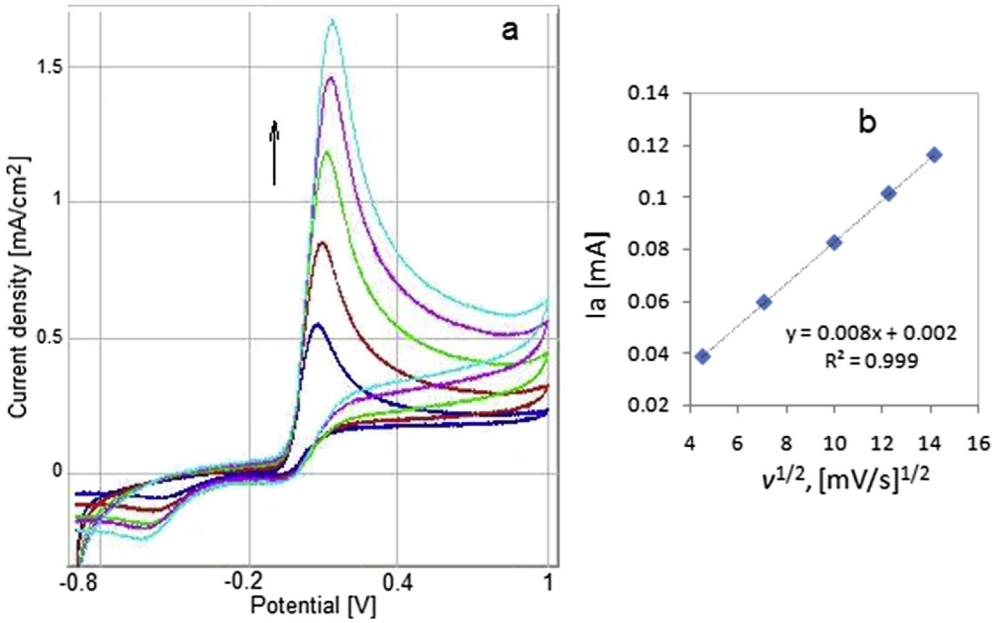

Fig. 16. Influence of the scan rate on the response of the GC/20cycl.MnTTPCl electrode in solution of 2.8 mM AA; scan rates: 20, 50, 100, 150, and 200 mV/s (a); linear dependence between the anodic current and the square root of the scan rate (b).

KCl 0.1 M and the calibration curve for AA concentrations between 0.14 and 11.34 mM are presented in Fig. 14.

The stability of the GC/20cycl.MnTTPCl electrode to more electro-oxidation processes was tested after washing it with distilled water and reimmersing into the electrolyte without any content of AA. The results, as presented in Fig. 15, show that the signal for AA is present only for the first scan, proving that the process is not irreversible and the modified electrode can be several times reused.

The influence of the scan rate on the response of the GC/20cycl.MnTTPCl electrode was determined in the case of 2.8 mM AA oxidation. The shape of the cyclic voltammetry (CV) and the linear dependence between the anodic current and the square root of the scan rate are represented in Fig. 16. The linear ascendant trend of this dependence is indicating that the process is solely electrochemical and controlled by diffusion.

By adding AA to the electrode modified with successive thin layers of Mn porphyrin and nanogold (GC/20cycl.MnTTPCl/n-Au), the oxidation peak of AA is preserved at the same potential but the current density is significantly increased (Fig. 17). This is in agreement with the results obtained during optical investigations.

The gold modified GC electrode (GC/n-Au) exposed to increased concentrations of AA gives an oxidation peak around 500 mV (Fig. 18).

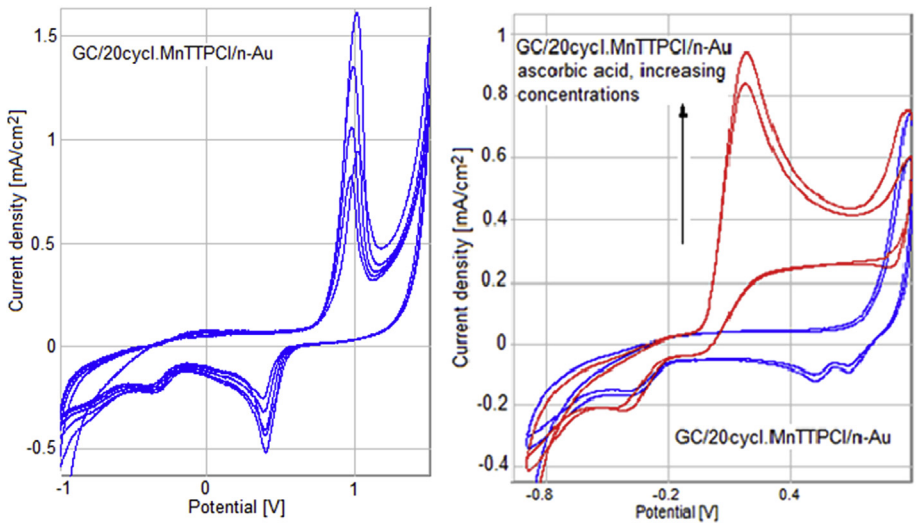

Fig. 17. Cyclic voltammograms for the GC/20cycl.MnTTPCl/n-Au electrode in a buffer solution 0,1 M PBS/0,1 M KCl (blue) and after adding of AA (red).

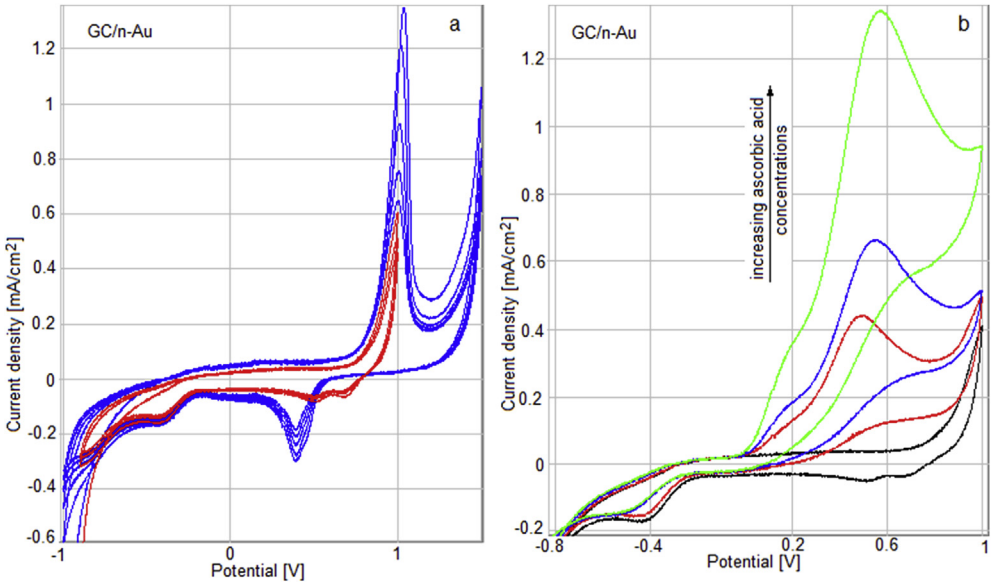

Fig. 18. Cyclic voltammograms for the GC/n-Au electrode in a buffer solution 0,1 M PBS/0,1 M KCl (a) and after successive adding of AA: 25, 50, and 100 μL (b).

The potential is shifted to more positive values as the AA concentration is increasing. The current density variation is proportional to AA concentration.

A comparison of the responses to AA oxidation of the Mn porphyrin and nanogold modified GC electrodes, namely, GC/20cycl.MnTTPCl, GC/n-Au/20cycl.MnTTPCl, GC/20cycl.MnTTPCl/n-Au, and GC/n-Au is presented in Fig. 19 for the same AA concentration. Analyzing Fig. 19, it can be concluded that MnTTPCl has a remarkable electrocatalytic activity toward AA oxidation proven both by the most negative potential and the highest current density.

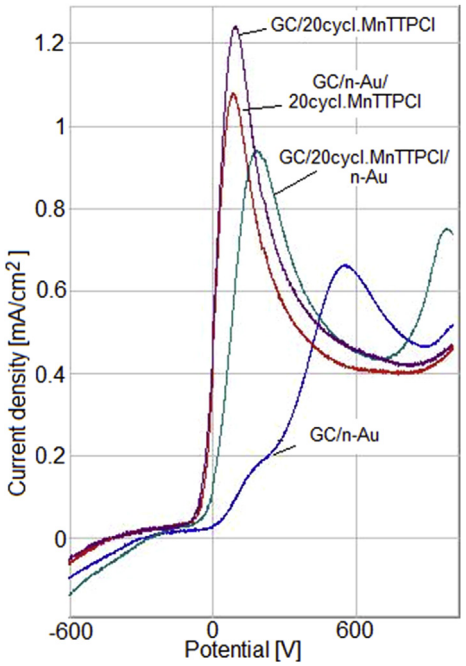

Fig. 19. Superimposed responses of the modified GC electrodes: GC/20cycl.MnTTPCl, GC/n-Au/20cycl.MnTTPCl, GC/20cycl.MnTTPCl/n-Au, and GC/n-Au to AA oxidation.

4. Conclusions

The amount of AA contained in biological fluids can be used to determine the oxidative stress in human metabolism. Excessive oxidative stress is linked to diabetes, cancer, and hepatic or coronary diseases. A deficiency of the antioxidant AA vitamin plays an important role in patients with porphyria cutanea tarda. For the facile detection of AA, porphyrin-based electrochemical sensors were conceived and tested [1,19,21].

This work is focused on the developments concerning new hybrids based on Mnmetalloporphyrin and gold colloids destined for the facile and readily detection of AA in the relevant range for medical investigations using UV–vis and electrochemical detection.

A comparison among the behavior of bare manganese-porphyrin, gold colloid alone, and their hybrid evidently shows that the gold colloid alone is not able to detect AA by UV–vis optical method; bare Mn porphyrin has two different behaviors depending on the AA concentration, probably because of the rate of coordination between AA and the Mn core of the porphyrin; the hybrid material (MnTTPCl/n-Au) has the best capacity to detect micromolar concentrations of AA in the range of physiological importance for human health. The detectable domain of concentration offered by this hybrid material varies from 2.6×10^{-6} to 4.38×10^{-5} M. It can be concluded that the MnTTPCl component in the hybrid is the determining factor for the detection capacity of AA. Although the gold colloid cannot detect AA on its own, its contribution to the widening and stabilizing of the plasmon absorption band of the MnTTPCl/n-Au hybrid for UV–vis detection cannot be neglected.

In addition, modified GC electrodes were obtained by thin film deposition of MnTTPCl, n-Au alone and in successive mixed thin films, comparing their response during the electrochemical oxidation of AA. The electrocatalytic effect of the MnTTPCl on the AA oxidation is justified both by the increase in the peak current density and the shift toward more negative potentials (0.024 V). Besides, the properties of the deposited film can be controlled by varying the number of scan cycles during deposition. The GC/MnTTPCl electrode has the best electrocatalytic effect for the AA oxidation and is promising for sensor applications.

Acknowledgments

The authors from Institute of Chemistry Timisoara of Romanian Academy are kindly acknowledging the support from Program 3-Porphyrins/2017 and from UEFISCDI PN III-ProgrammeCorOxiPor 107PED/2017. The authors from INCDEMC gratefully acknowledge financial support from PN 09-34 04 04.

References

[1] C. Wang, R. Yuan, Y. Chai, S. Chen, Y. Zhang, F. Hu, M. Zhang, Electrochim. Acta 62 (2012) 109.
[2] J.M. May, Subcell. Biochem. 56 (2012) 85.
[3] M.N. Diaz, B. Frei, J.A. Vita, J.F. Keaney Jr., N. Engl. J. Med. 337 (1997) 408.
[4] S. Kojo, Curr. Med. Chem. 11 (2004) 1041.
[5] M. Valko, H. Morris, M.T. Cronin, Curr. Med. Chem. 12 (2005) 1161.
[6] A.M. Pisoschi, A. Pop, Eur. J. Med. Chem. 97 (2015) 55, http://dx.doi.org/10.1016/j.ejmech.2015.04.040.
[7] A.R. Ness, F.P. Cappucio, R.W. Atkinson, K.-T. Khaw, D.G. Cook, Int. J. Epidemiol. 28 (1999) 450.
[8] A.M. Pisoschi, A. Pop, A.I. Serban, C. Fafaneata, Electrochim. Acta 121 (2014) 443.
[9] K.E. Anderson, Hepatology 45 (2007) 6.
[10] V.A. Percy, D. Naidoo, S.M. Joubert, R.J. Pegoraro, S. Afr. J. Med. Sci. 40 (1975) 185.
[11] N. Dąbrowska, A. Wiczkowski, Adv. Clin. Exp. Med. 26 (2017) 155.
[12] R. Kand'ár, P. Záková, J. Sep. Sci. 31 (2008) 3503.
[13] M. Levine, S.J. Padayatty, M.G. Espey, Adv. Nutr. 2 (2011) 78.
[14] D.H. Fadhe, J. Al-Nahrain Univ. 15 (2012) 88.
[15] N. Donato, D. Aloisio, S.G. Leonardi, M. Latino, G. Neri, AISEM Annual Conference, 2015, http://dx.doi.org/10.1109/AISEM.2015.7066821, XVIII.
[16] J. Du, R.R. Yue, F.F. Ren, Z.Q. Yao, F.X. Jiang, P. Yang, Y.K. Du, Biosens. Bioelectron. 53 (2014) 220.
[17] X. Zhu, T. Zhao, Z. Nie, Y. Liu, S. Yao, Anal. Chem. 87 (2015) 8524.
[18] H. Cheng, X. Wang, H. Wei, Anal. Chem. 87 (2015) 8889.
[19] M. Lucero, M. Riquelme, G. Ramírez, M.C. Goya, A.G. Orive, A.H. Creus, M.C. Arévalo, M.J. Aguirre, Int. J. Electrochem. Sci. 7 (2012) 234.
[20] T. Skeika, C. Marcovicz, S. Nakagaki, S.T. Fujiwara, K. Wohnrath, N. Nagata, C.A. Pessoa, Electroanalysis 19 (2007) 2543.
[21] J.C. Kemmegne-Mbouguen, L. Angnes, Sens. Actuators B Chem. 212 (2015) 464.
[22] T. Weitner, A. Budimir, I. Kos, I. Batinic-Haberle, M. Birus, Dalton Trans. 39 (2010) 11568.
[23] S. Sun, D. Wu, Q. Wei, Y. Han, X. Chen, Y. Shen, P. Zhu, B. Du, J. Fluoresc. 19 (2009) 809.
[24] E. Fagadar-Cosma, M.C. Mirica, I. Balcu, C. Bucovicean, C. Cretu, I. Armeanu, G. Fagadar-Cosma, Molecules 14 (2009) 1370.
[25] A.D. Adler, F.R. Longo, F. Kampas, J. Kim, J. Inorg. Nucl. Chem. 32 (1970) 2443.
[26] E. Fagadar-Cosma, C. Enache, I. Armeanu, D. Dascalu, G. Fagadar-Cosma, M. Vasile, I. Grozescu, Mater. Res. Bull. 44 (2009) 426.
[27] P. Muthukumar, S. Abraham John, J. Colloid Interface Sci. 421 (2014) 78.
[28] I. Sebarchievici, B.O. Tăranu, M. Birdeanu, S.F. Rus, E. Făgădar-Cosma, Appl. Surf. Sci. 390 (2016) 131.
[29] I.V. Sazanovich, V.A. Galievsky, A. van Hoek, T.J. Schaafsma, V.L. Malinovskii, D. Holten, V.S. Chirvony, J. Phys. Chem. B 105 (2001) 7818.
[30] C.J. Medforth, M.O. Senge, K.M. Smith, L.D. Sparks, J.A. Shelnutt, J. Am. Chem. Soc. 114 (1992) 9859.
[31] C. Ünaleroğlu, Y. Mert, B. Zümreoğlu-Karan, Inorg. Metal-Org. Chem. 31 (2001) 1531.
[32] M.R. Mucalo, K.M. Babu, K.S.W. Wu, J. Colloid Interf. Sci. 310 (2007) 184.
[33] I. Creanga, A. Palade, A. Lascu, M. Birdeanu, G. Fagadar-Cosma, E. Fagadar-Cosma, Dig. J. Nanomat. Biostructures 10 (2015) 315.
[34] M. Veyrat, O. Maury, F. Faverjon, D.E. Over, R. Ramasseul, J.C. Marchon, I. Turowska-Tyrk, W.R. Scheidt, Angew. Chem., Int. Ed. 33 (1994) 220.
[35] C.C. de Melo, W. da Conceição Moreira, T.J. Martins, M.R. Cordeiro, J. Ellena, F.F. Guimarães, F.T. Martins, J. Mol. Struct. 1076 (2014) 468.
[36] A.O. Okunola, T.C. Nagaiah, X. Chen, K. Eckhard, W. Schuhmann, M. Bron, Electrochim. Acta 54 (2009) 4971.
[37] L. Gaillon, F. Bedioui, J. Devynck, J. Electroanal. Chem. 303 (1991) 283.
[38] C.-F. Zhang, M. Chen, C. Nakamura, J. Miyake, D.-J. Qian, Langmuir 24 (23) (2008) 13490.
[39] N.S. Trofimova, A.Y. Safronov, O. Ikeda, Electrochim. Acta 50 (2005) 4637.
[40] C.-F. Zhang, M. Chen, D.J. Qian, Thin Solid Films 517 (2009) 3760.